Available online at www.sciencedirect.com
ScienceDirect
Polymer 48 (2007) 4558–4566
polymer
www.elsevier.com/locate/polymer

Dielectric spectroscopy of poly(butylene succinate) films

Horng-Jer Tai*

Department of Chemical Engineering, I-Shou University, No. 1, Hsueh-Cheng Road, Sec. 1, Ta-Hsu Hsiang, KaoHsiung County 84008, Taiwan

Received 30 January 2007; received in revised form 17 May 2007; accepted 18 May 2007
Available online 24 May 2007

Abstract

Dielectric properties of poly(butylene succinate) crystallized under different conditions have been reported in the temperature range of 163–383 K and in the frequency range of $0.01-10^5$ Hz. Both the dipolar α and β processes have been identified at low temperatures: the α process is associated with the amorphous fraction while the β with the relaxations in both the amorphous and crystalline fractions. The space charge effect dominates the high temperature dielectric spectra. These spectra have been analyzed in the light of an equivalent circuit model. The Maxwell–Wagner–Sillars polarization, electrode polarization and free charge motion are well resolved. At 383 K, near the melting temperature (387 K), massive melting and subsequent recrystallization have been observed. The peculiar evolution of the spectra is also analyzed using the same equivalent circuit model. The relationship between the fitting parameters and the evolved microstructures is discussed.

Keywords: Dielectric spectroscopy; Poly(butylene succinate); Crystallization

1. Introduction

Poly(butylene succinate), PBSu, is a biodegradable synthetic aliphatic polyester. It can be found in packaging film, bags, flushable hygienic products, and garden mulch. It has a similar melting range as that of low density polyethylene, so can be processed on conventional equipments commonly used for polyolefins [1]. In order to promote its application in various fields, more studies are needed to achieve a better understanding, especially in the material processing aspect. PBSu has two polymorphs – the α and β crystal forms. The latter can be found only when the material is under strain. The transition between these two forms occurs reversibly under the application and removal of strain. Both forms are of monoclinic crystal system, but have different lattice parameters, which are attributed to the different conformations in the tetramethylene unit [2–5]. PBSu exhibits an interesting multiple melting behavior, which invoked many thermal investigations. Yoo and Im studied the melting behavior of isothermally crystallized PBSu using differential scanning calorimetry and X-ray diffraction and suggested there existed two morphologically different crystallites, and that simultaneous melting and recrystallization occurred [6]. A study on nonisothermally crystallized PBSu using DSC and temperature modulated DSC by Qiu et al. also came to a similar conclusion [7]. Yasuniwa and Satou study the melting–recrystallization behavior of PBSu resins of three different molecular weight distributions and reported that the height of the high temperature melting peak decreased with increasing molecular weight, whereas that of the low temperature one increased [8]. It was attributed to the lower recrystallization rate for the higher molecular weight polymers.

Relaxation properties are very important in polymer processing. Many processes are characterized as being elastic, while others as viscous. Many products, such as shrink films and foams, make use of materials in their unrelaxed state. Relaxation properties can be best studied by dynamic mechanical spectroscopy, dielectric relaxation spectroscopy (DRS) or NMR spectroscopy. Relaxation processes play a dominant role and result in a complex pattern of temperature and

* Tel.: +886 7 6578901; fax: +886 7 6578945.
E-mail address: hjtai@isu.edu.tw

0032-3861/$ - see front matter © 2007 Elsevier Ltd. All rights reserved.
doi:10.1016/j.polymer.2007.05.043

time/frequency-dependent properties [9]. For polymers in the solid (crystalline or amorphous) state or in the viscoelastic liquid state, the way of molecular packing is of great importance in determining the relaxation behavior. Structural transitions in polymers are generally accompanied by changes in relaxation properties. When an oscillatory electric field is applied to a polymeric material, several types of polarization are operative: electronic, ionic, orientational and space charge. A dielectric spectrum is a complicated manifestation of the combination of these operative polarization sources. Orientational and space charge polarizations are particularly important when structural transitions are concerned. For a polymer, many relaxatory modes are involved in orientational polarization. They can be grouped into local processes, cooperative processes in longer chain sequences, chain diffusion (flow) and specific processes in semicrystalline states [9]. Polymers exhibit thermorheological complexity: different relaxation processes contribute to viscoelasticity which shows different temperature dependences [10]. Reported DRS studies on PBSu are scarce. However, much has been done on poly(ethylene terephthalate), PET, a more popular member in the thermoplastic polyester family. PET has the advantage that it can be prepared in a completely amorphous state as well as in a semicrystalline state. The loss curve in a dielectric loss–frequency plot becomes much broader for semcrystalline PET than that for an amorphous specimen; the relaxation times are much longer and their distributions are much broader. The Maxwell–Wagner–Sillars (MWS) interfacial polarization effect can also be seen in the dielectric permittivity curve for the two-phase semicrystalline polymer, which is absent for its amorphous counterpart [11]. No specific crystalline relaxation process was reported for PET. This process had been reported for semicrystalline polyvinyl alcohol. DRS can be applied to monitor a crystallization process. Fukao and Miyamoto reported that the segmental relaxation during slow cold crystallization near the glass transition temperature in PET experienced a change in relaxation modes: the relaxation function changed from a Kohlrausch–Williams–Watts equation in the amorphous state to a Cole–Cole equation in the semicrystalline state [12]. The space charge-related effects in biaxially stretched PET films were studied by Neagu et al. [13]. They found that the DC conductivity followed the Vogel–Fulcher–Tammann (VFT) equation and concluded that the charge carrier transport mechanism is governed by the motion of the polymer chains. It is very interesting to see how this biodegradable polymer behaves in the DRS experiment. In this study, we explore the relaxation properties of PBSu and seek to correlate them with the polymer crystalline structure.

2. Experimental

2.1. Materials

The PBSu resin used in this study was Bionolle #1001 supplied by Showa Highpolymer Co. Ltd, and its chemical structure is shown in Scheme 1. It has a melt flow rate of 1 g/10 min at 190 °C and melting and glass transition temperatures of 387 and 241 K, respectively [3]. Its $\overline{M}_w$ is 160,000 g/mole and its $\overline{M}_n$ is 35,000 g/mole [1,3]. The resin was used as-received.

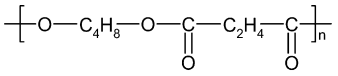

Scheme 1. Chemical structure of poly(butylene succinate).

2.2. Sample preparation and analysis

The PBSu pellets were dried at 343 K for 4 h and then melt processed at 453 K for 3 min using a Brabender Plasti-Corder PL2000 equipped with roller blade rotors. The melts were transferred to a compression molding machine which was preset at the same temperature. After the melts were heat pressed into films for 3 min, the heating platens were water-cooled to 363 K. The films were allowed to crystallize at 363 K for 2 h. Films of thicknesses of about 100 μm were thus prepared. DRS measurements in the frequency range of 10–0.1 MHz were carried out by means of a TA Instruments DEA 2970 dielectric analyzer equipped with a liquid nitrogen cooling system. The ceramic parallel plate sensor was employed and the specimen size was 26×26 mm^2. Three different DRS experimental methods were used. The first was to study the dielectric behaviors for the previously prepared 363 K crystallized samples. The specimens were firstly cooled down to 163 K and then scanned isothermally using a temperature step/frequency sweep method and measurements were taken every 10 K over the temperature range between 163 and 363 K. The second was to study the dielectric behaviors for the quenched PBSu samples. The procedure here was the same as that adopted by Yoo et al. [6] to obtain amorphous samples for the cold crystallization study. At first, the specimens were held at 423 K for 0.5 h to achieve complete melting. Next, the specimens were quenched down to 163 K with liquid nitrogen and then treated with the same experimental steps used for the 363 K crystallized samples. The third was to study the dielectric behaviors for the recrystallized samples: the 363 K crystallized specimens were heated directly up to 383 K and held at that temperature for 7 h, during which continuous isothermal frequency sweep measurements were taken.

3. Results and discussion

3.1. α and β relaxations

The isothermal plots for the permittivity, ε', and the loss factor, ε'' vs. frequency of the 363 K crystallized PBSu samples in the temperature range 163–363 K are shown in Figs. 1 and 2, respectively. In order to better demonstrate their features, curves of temperatures of 163–263 K are shown in a semilog format, while curves of temperatures of 273–363 K are shown in a log–log format. At low temperatures (Fig. 2(a)), we see an extremely broad relaxation peak in ε'' that becomes narrower and moves toward the high frequency

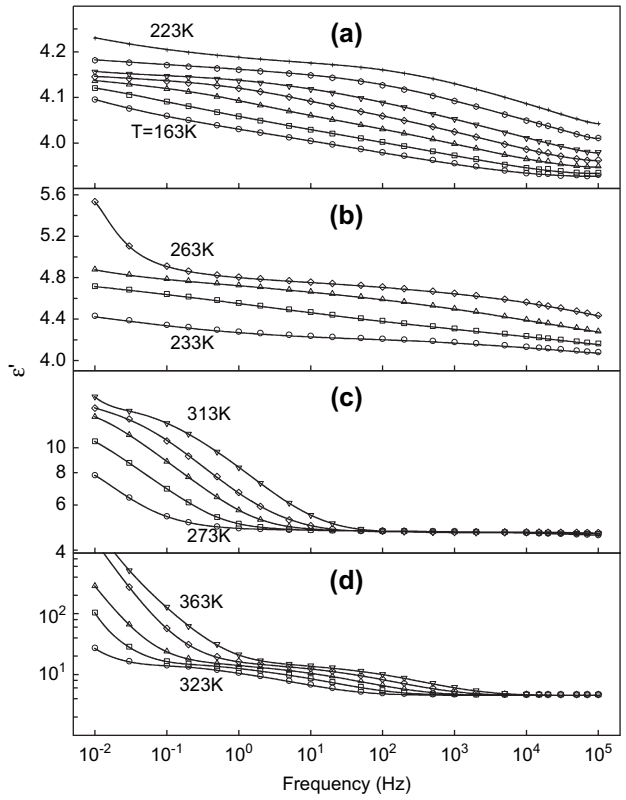

Fig. 1. Dielectric (relative) permittivity spectra of the 363 K crystallized PBSu films at various temperatures. Solid curves are drawn through the data to guide the eye.

side as the temperature increases. In Fig. 1(a), we can also see the corresponding slow transition steps in the ε' curves. This is the subglass β transition process, which can be identified more easily as the spectra were presented in an isochronal format later. The origin of this process is not clear yet, some authors assigned it to a reorientation of the ester groups [14,15]; others believed it to be related to the torsional vibrations of main chains in the neighborhood of its local equilibrium conformation [16]; still others thought it to be involved with certain conformation sequence transitions [17]. It seems that this broad peak is constituted of several individual peaks which are contributed from different components of the material. Burshtein et al. had presented in thermotropic linear polyesters relaxational transitions which could be resolved as two peaks with two different relaxation times and were attributed to the motion of ester groups in the amorphous and crystalline regions, respectively [15]. Since there is no well-defined peak which can be assigned positively to either amorphous, crystalline or intermediate phases in these figures, here it is difficult to use curve fitting techniques to resolve these individual peaks unbiasedly. However, the low-frequency portion of this composite peak is believed to be contributed from the slower relaxation processes originated from the crystalline component (see discussions on Figs. 3 and 4). This low-frequency portion shifts much faster than the composite peak, indicating that the β motions in the crystalline phase are controlled by a different mechanism. Lattice vibrations, which provided the free space needed for the dipoles to oscillate with the applied field,

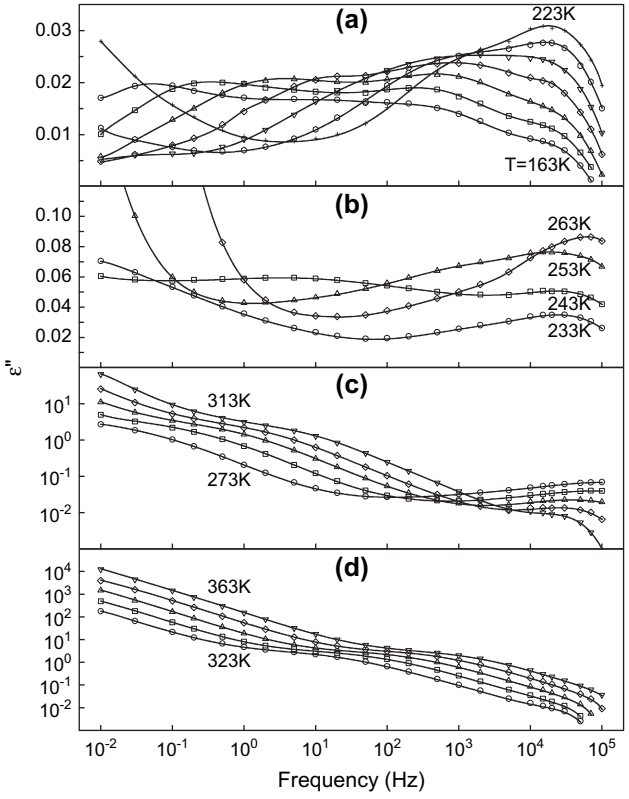

Fig. 2. Dielectric loss spectra of the 363 K crystallized PBSu films at various temperatures. Solid curves are drawn through the data to guide the eye.

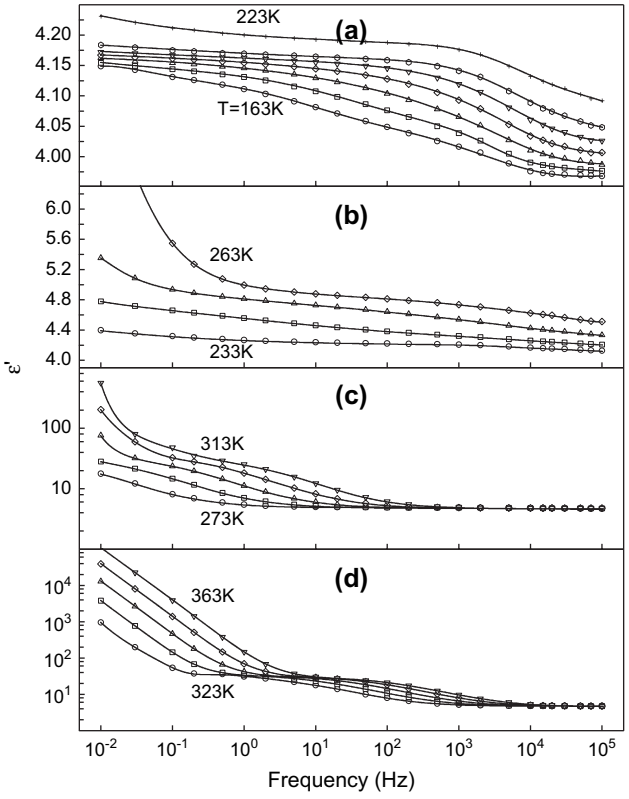

Fig. 3. Dielectric (relative) permittivity spectra of the quenched PBSu films at various temperatures. Solid curves are drawn through the data to guide the eye.

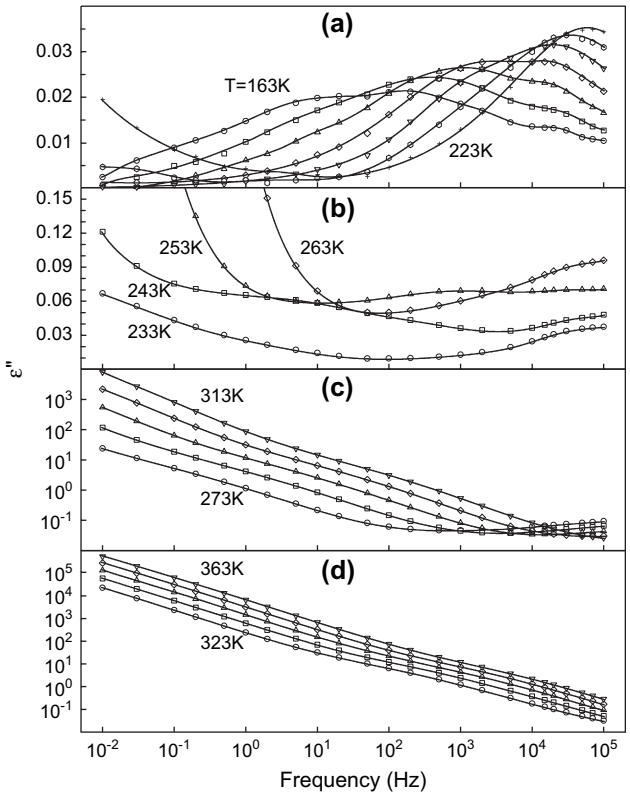

Fig. 4. Dielectric loss spectra of the quenched PBSu films at various temperatures. Solid curves are drawn through the data to guide the eye.

could be the cause. When the temperature is raised, thermal fluctuations with higher frequencies and amplitudes relax the constraints imposed upon the crystalline component; the β motions become less correlated and relax at a similar rate as those β dipoles in the amorphous component, wherein the β motions are local in nature. As the β processes merge into a narrower peak with increasing temperature, another relaxation process become evident at the low-frequency end in the curves for 213 and 223 K (Fig. 2(a)). This is the α process which is related to the segmental mobility. This process can be best observed in Figs. 1(b) and 2(b) when one compares the dielectric behaviors among the 233–263 K ε' and ε'' curves: with increasing temperature, a peak (in ε'') moves fast from a frequency 10^{-2} Hz to 10^{4} Hz and a step change in ε' behaves similarly. The observation of the rapid shifting of the loss maximum frequency of the α relaxation with increasing temperature at temperatures above T_g is not unusual [18]. Afterwards, it often merges with the β process. The α dielectric response function is greatly influenced by the effects related to space charge activities on the low-frequency side and the broad β processes on the high frequency side; hence one can not see clear-cut features of this process in the plots.

The space charge effects are evident in Fig. 2(b): the 253 and 263 K ε'' values increase dramatically at low frequencies with decreasing frequency. It is also interesting to note that these effects become evident only when the temperature is raised higher than T_g (241 K). At temperatures higher than 263 K, growths in ε' with decreasing frequency (Fig. 1(c)) are observed. DC conduction alone will not affect the behavior in ε', and the slope of a log ε''–log f plot for low-frequency ε'' values at 263 K is −0.65, instead of −1. The high values of ε'' in Fig. 2(c) do not correspond to the intrinsic dipolar loss characteristic of PBSu. A relaxation process other than dipolar ones sets in, which must have something to do with the mobilization of space charges. It is assigned to a Maxwell–Wagner–Sillars (MWS) interfacial polarization process, which originates from the charge build-up created by contact of two phases of different charge conductivity. This relaxation can be better identified in the ε' plots than in the ε'' plots where the relaxation was masked by the DC conduction loss. In Fig. 1(c), step-like transitions in ε' can be easily identified, especially for the 303 and 313 K curves. While for ε'' curves, relaxation shoulders instead of relaxation peaks, caused by joint contributions from a MWS polarization and DC conduction, are observed. At these temperatures, the unmasked dipolar behaviors can only be observed at frequencies higher than 10^{4} Hz in Fig. 2(c), where dipolar relaxation peaks shift toward the high frequency end with increasing temperatures. At temperatures higher than 313 K, both ε' and ε'' exhibit extremely high values at low frequencies (Fig. 2(c) and (d)). Similar features can be seen: a MWS plateau at 10–100 Hz along with a steep ascent with decreasing frequencies. When ε' and ε'' for the same temperature are plotted together, the low-frequency portions are not parallel to each other. The dispersion in ε' indicates the existence of another relaxation process at frequencies lower than those where the MWS relaxation takes place. This rather slow process is assigned to an electrode polarization. The molecular reason for this polarization is the blocking of space charges at the sample/electrode interface, which results in a build-up of space charges within the sample adjacent to the electrodes. The associated capacitance and complex admittance for this electrical double layer are large and the effect increases with decreasing frequency [19]. The low-frequency slopes of the ε'' curves in Fig. 2(d) are close to −1, implying that the electrode polarization contribution to ε'' is masked by the DC conduction loss due to the strong DC conductivity at high temperatures.

In comparison, Figs. 3 and 4 are the ε' and ε'' plots of the quenched PBSu samples. If compared with the 163 K curve in Fig. 2(a), the β relaxation peak in Fig. 4(a) is much narrower. The low-frequency contribution to ε'' disappears; that is why we attribute the low-frequency portion of the broad composite β relaxation peak in Fig. 2(a) as contributed from the crystalline component of the 363 K crystallized samples. The dispersion features in Fig. 4(b) are similar to those shown in Fig. 2(b), except that the space charge effects are switched on earlier for the quenched samples: the low-frequency upswing in ε'' can be clearly identified for 243 K curve and but can not be seen in Fig. 2(b); the steep upswings in ε'' start at higher frequencies for the 253 and 263 K curves, as compared to their counterparts in Fig. 2(b). Similar peculiarities can also be found if we compare Fig. 3(b) with Fig. 1(b). In Figs. 3(c) and (d) and 4(c) and (d), we also see higher ε' and ε'' values than those shown in Figs. 1 (c) and (d) and 2(c) and (d) because of the fact that charge carriers are more

mobile in the less crystalline matrix and space charge effects are more prominent at higher temperatures. We see step-like growths in ε' with decreasing frequency in Fig. 3(c) around 10^{-2}–10^{2} Hz and in Fig. 3(d) around 1–10^{4} Hz. This is the MWS process as pointed out previously. This MWS process is less distinctive in ε'' (compared to that in Fig. 2(c)) because it is blurred by the higher and earlier DC conduction and electrode polarization effect. The value of the low-frequency $\log \varepsilon''$–$\log f$ slope in Fig. 4(c) is -0.68, indicating that the electrode polarization has already taken place. The extremely high ε' values at low frequencies in Fig. 3(d) are also manifestations of the electrode polarization effect. The values of the low-frequency slopes of the ε'' curves in Fig. 4(d) are close to -1, which is also seen in Fig. 2(d). Again, in the loss spectra, the strong DC conductivity at high temperature overshadows the electrode polarization contribution.

Concerning about the features of the α and β relaxations, it is more revealing when the dielectric spectra are presented in an isochronal format. Fig. 5(a)–(c) presents the isochronal ε'' plots for both the 363 K crystallized and the quenched samples at 50, 500 and 5000 Hz, respectively. We see sharper α relaxation peaks with higher relaxation strengths and broader but weaker β relaxation peaks. Clearly, both the α and β relaxations become resolved much better. The separation between these two relaxations is better for the quenched samples. Only when at frequencies lower than 50 Hz can the β peak for the 363 K crystallized samples be resolved better. Compared with the results for the 363 K crystallized samples, the β peak for the quenched samples displaces at a higher rate; the space charge effects on the α peak are also more prominent. The shapes of the α peak for these two kinds of samples look similar. The minor differences in the shape and position come from a combination of more pronounced space charge effects on the quenched samples on the high temperature side and more overlapping of the β peak for the 363 K crystallized samples on the low temperature side. At frequencies much higher than 5000 Hz in the isochronal ε'' plots, the two relaxation peaks tend to merge together and only the α peak can be clearly identified.

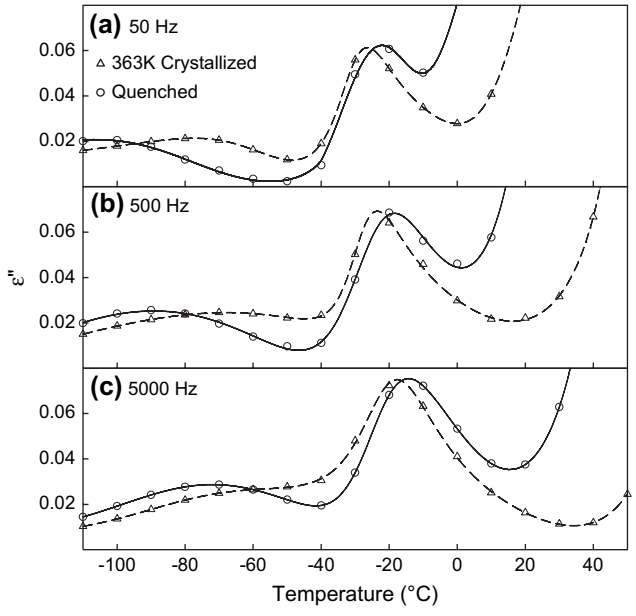

Fig. 5. Isochronal plots of ε'' for both the 363 K crystallized and the quenched samples at the indicated frequencies. The lines are drawn through the data to guide the eye.

The peak positions, that is the temperatures at which the ε'' values are at their local maxima, of the two relaxations are retrieved from these isochronal plots and presented in the Arrhenius plot of Fig. 6. The f_{max}, which represents the local maximum position in an isothermal plot, in Fig. 6 is actually the specified frequency at which the isochronal plot is made. The abscissa in Fig. 6 is constructed with the interpolated temperatures obtained from the local maxima in the isochronal plots. The dielectric β processes obey an Arrhenius temperature dependence typical of a subglass transition process. The activation energy for the quenched samples is estimated to be 10.2 kcal/mol, which agrees very well with those reported for aliphatic polyesters in the literature (9–13 kcal/mol) [16,17,20–22]. The activation energy for the 363 K crystallized samples was considerably higher, of a value 18 kcal/mol. The β relaxation has contributions originated from the crystalline fraction and is of a more correlated nature. We speculate that this is related somehow with the lattice vibrations in the crystalline fraction; and at higher temperatures, the lattice vibrations become so violent that the structure is open for the local β process that it eventually merge with that in the amorphous fraction (see Figs. 2(a) and 4(a)). The curves for the α process are curvilinear and follow the Vogel–Fulcher–Tammann form. The apparent Arrhenius activation energies were estimated to be 43.2 and 46.3 kcal/mol for the quenched and 363 K crystallized samples, respectively. Actually the two curves are very close to each other. Taking the DC conduction effect and the overlapping β contributions into account, the relaxation peak positions for the two kinds of samples can be considered as nearly identical.

3.2. MWS and electrode polarizations

Among the DRS features of PBSu, the prominent interfacial MWS polarization is especially interesting. It is related

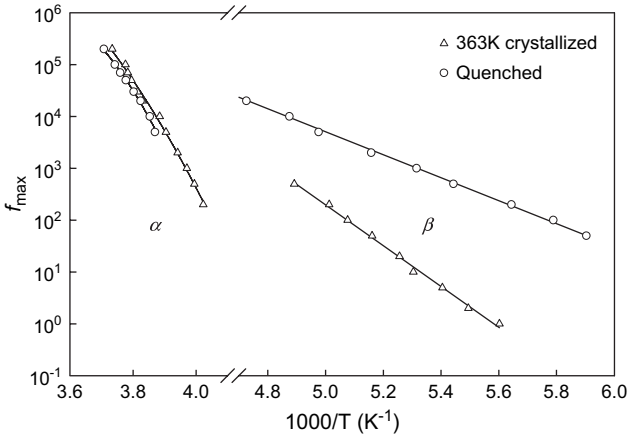

Fig. 6. Arrhenius plots of the α and β processes for both the 363 K crystallized and the quenched samples.

to the difference in the mobility of charge carriers between the two phases within the matrix. Since the working experimental electric field is only 10^4 V/m and under an AC condition, charge carrier injection is not likely to happen. The charge carriers may originate from the additives in the commercial resin. The characteristic MWS relaxation frequency reflects the time scale of rearrangements of the charges [23]. The behaviors of MWS relaxation depend strongly upon the geometry of the interface or the shape and size of the dispersed phases [24]. For a quantitative analysis of the complex dielectric spectra of the MWS process and also to account for the electrode polarization process, we have adopted an equivalent circuit model, which contains a Cole–Cole (CC) distributed element and a constant phase-angle (CPA) element, to fit the frequency dependence of the isothermal complex dielectric function. The fitting job was done with the complex nonlinear least squares frequency-response fitting software LEVMW developed by Macdonald [25]. The equivalent circuit model and related formula are explained in Appendix section. The fitting was restricted to the spectra within the temperature range between 303 and 363 K because isothermal curves were less complicated in this range, and within the frequency between 0.01 and 10,000 Hz to avoid the complication from the dipolar processes that were still present at high frequencies. The fitting was also restricted to the spectra of the 363 K crystallized samples only, because the morphology of the quenched samples would change in this temperature range due to recrystallization. Fig. 7 shows the comparison of the experimental and fitted ε' and ε'' curves and Table 1 lists the fitted parameters. As the temperature increases, the behavior of the CPA element changes from being purely capacitive ($\phi \approx 1$ at 303 K) to more resistive ($\phi = 0.7$ at 363 K). Non-uniform current and potential distributions exist between the electrodes and a semi-crystalline polymeric sample because of the large difference in the conductivity between the amorphous and crystalline regions. The non-uniform current and potential distributions on the electrodes lead to a distributed and frequency-dependent Ohmic resistance [26]. At high temperatures, the sample bulk conductivity (σ_o in Table 1) becomes stronger and the resultant potential difference becomes higher accordingly, which leads to an electrode polarization with a more prominent mixed capacitive-resistive behavior.

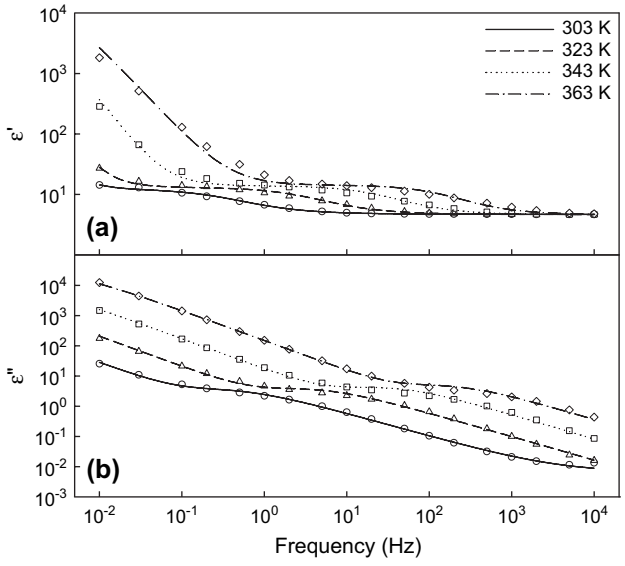

Fig. 7. Phenomenological data-fitting for the 363 K crystallized PBSu films. Symbols are experimental, curves are calculated using the model described in Appendix and parameters of Table 1.

The intrinsic relaxation spectra for the sample itself are characterized by a combination of an MWS process and a DC conductivity effect. The relaxation strength, $\Delta\varepsilon$, for the MWS process grows with increasing temperature, as can be seen in Table 1. Charge carriers, which are trapped by the surrounding crystallites, accumulate at the interface and move through the amorphous phase under the influence of an applied voltage. These charge carriers are responsible for this relaxation, and the resultant relaxation strength is much stronger than those for dipolar processes. The mild increase in $\Delta\varepsilon$ implied that a higher amount of charge carriers are involved at higher temperatures. The mobility of these charge carriers should also increase with increasing temperature so that the relaxation time becomes shorter. The bulk conductivity in a polymer is closely related to ion mobility. The behaviors of the trapped charge carriers should resemble those of global charge carriers which are responsible for bulk conductivity. One interesting demonstration of this aspect is presented in Fig. 8. The Arrhenius plots of the reciprocal of the MWS relaxation time and of the bulk conductivity exhibit two parallel lines. For a more conductive spherical amorphous phase having a permittivity ε_2' and a conductivity σ_2 dispersed in a much less conductive crystalline matrix having a permittivity ε_1' and a conductivity $\sigma_1 \approx 0$, the MWS relaxation time can be expressed as [24]:

$$\tau_{\mathrm{MWS}} \approx \frac{\varepsilon_1' + (\varepsilon_2' - \varepsilon_1')/3}{\sigma_2/3}. \tag{1}$$

If we assume that these conditions can be applied to the PBSu samples and that the bulk conductivity σ is proportional to σ_2 according to the rule of mixtures, the MWS relaxation time and the bulk conductivity will be inversely correlated. The result depicted in Fig. 8 is in good agreement with the above deduction. The activation energies are 26.84 kcal/mol, which lie in between those for α and β relaxations. The ion mobility in polymer electrolytes is considered to be related to segmental motion of polymer chains [18,27,28]. Most of the ions move from one coordinating site to a neighboring site through the cooperative rearrangement of polymer segments. The Arrhenius (instead of VFT) nature of the line and the lower activation energy seems to indicate that the transport of these impurity ions is not highly associated with the movement of polymer chains and that the ions move in a more independent, less correlated manner.

3.3. Spectroscopic evolution at 383 K

The 363 K crystallized samples were further heated to 383 K and held isothermally for a long period of time so

Table 1
The fitting parameters for the equivalent circuit described in Appendix

T (K)	ε_∞	σ_o (S/m)	$\Delta\varepsilon$	τ (s^{-1})	α	A ($S\ s^{\phi}$)	ϕ
303	4.7	1.7×10^{-11}	8.0	4.5×10^{-1}	0.76	1.3×10^{-8}	0.93
313	4.7	4.2×10^{-11}	8.2	1.6×10^{-1}	0.76	8.4×10^{-8}	1.04
323	4.7	1.2×10^{-10}	8.6	4.7×10^{-2}	0.78	1.4×10^{-7}	1.04
333	4.7	3.3×10^{-10}	8.7	1.4×10^{-2}	0.82	1.4×10^{-7}	0.99
343	4.7	9.6×10^{-10}	9.5	5.5×10^{-3}	0.81	2.3×10^{-7}	0.88
353	4.7	3.0×10^{-9}	9.8	2.4×10^{-3}	0.77	2.4×10^{-7}	0.77
363	4.6	8.4×10^{-9}	10.3	1.0×10^{-3}	0.81	6.2×10^{-7}	0.70

that melting and recrystallization might occur. The evolving spectra are shown in Fig. 9. At the beginning ($t=0$ min), the spectrum manifested a completely different features from those obtained at low temperatures. We see a single relaxation process in the ε' spectrum and that the ε'' spectrum is dominated by a DC conductivity effect. As the time increases, an additional higher frequency ($\sim10^4$ Hz) relaxation process become evident in ε', and we can also see the parallel change in ε''. The final spectra ($t=405$ min) have features similar to those seen in Fig. 7. From the discussions in the above section, the relaxation at the lower frequency is identified as an electrode polarization process, and the higher frequency one as an MWS process. PBSu exhibits prominent melt-recrystallization behaviors [5–8]. According to Yasuniwa and Satou [8], intensive melting and recrystallization occur between 366 and 383 K. PBSu has a reported melting temperature of 387 K [4]. Yoo and Im [6] even reported a single melting peak at 391 K was obtained for melt crystallization at 388 K for long hours. At 383 K, extensive melting in the samples can be expected. However, 383 K is certainly not high enough for all the crystal seeds to be destroyed completely. Fig. 9 gives us clear evidences of simultaneous melting and recrystallization, a scheme proposed by many authors [5–8]. Melting and recrystallization are competing with each other; recrystallization is more dominant at low temperatures while melting is more dominant at higher temperatures. The samples experienced extensive melting at the beginning ($t=0$), and after about 400 min, the slow recrystallization process had finally come to an end.

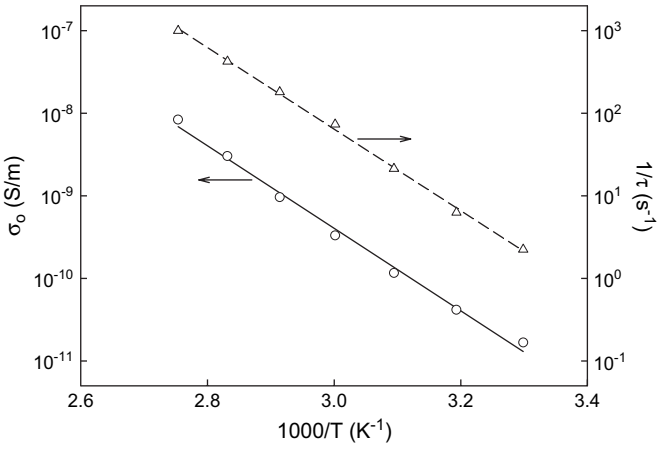

Fig. 8. Arrhenius plots of the bulk conductivity (σ_o) and the reciprocal of the CC relaxation times (τ) for the MWS process for the 363 K crystallized films.

Using the same fitting equivalent circuit model as described in Appendix section, the fitted parameters are depicted in Fig. 10. The parameters A and ϕ for the CPA element which simulates the electrode polarization behavior are relatively stable throughout the whole period. However, the parameters for the elements which represent the intrinsic material behaviors did vary to higher extents in systematic manners but the patterns of change are different for each of these parameters. The bulk conductivity, σ_o, and the relaxed dielectric constant, ε_∞, are both decreasing functions of recrystallization time. The reduction of the more conductive amorphous fraction results in a decrease in the bulk conductivity, while the increase in crystalline fraction makes parts of dipoles inactive for polarization as they are locked inside. The MWS relaxation strength, $\Delta\varepsilon$, experiences the most dramatic change among these parameters and also levels earliest. The appearance of this curve is reminiscent of crystallization conversion curves in kinetic studies. If we accept the assumption that $\Delta\varepsilon$ is proportional to the amount of trapped charge carriers in the amorphous region surrounded by the closed crystalline matrix, then the change in $\Delta\varepsilon$ can be taken to represent the degree of spherulitic conversion from the melt. The MWS relaxation time, τ, also increases with recrystallization time, and it continues to increase after $\Delta\varepsilon$ have leveled off. The continuous increase suggests that the internal structure is constantly changing, until

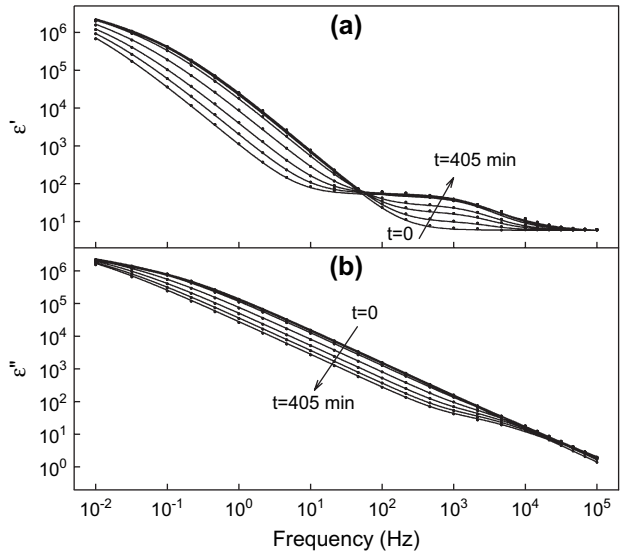

Fig. 9. Evolution of the dispersion spectra during the 383 K isothermal recrystallization of the 363 K crystallized PBSu films. Symbols are experimental, solid curves are the best fits to the model described in Appendix.

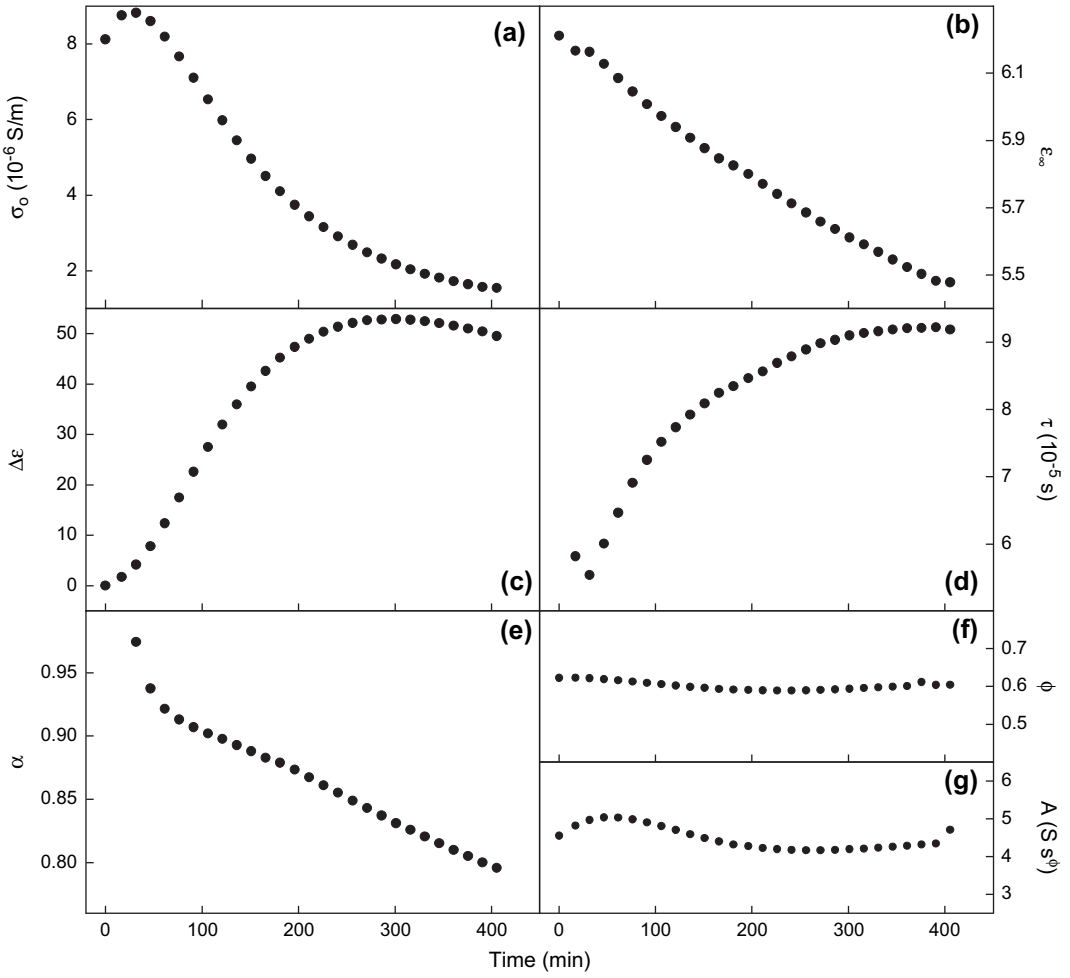

Fig. 10. Variations of model parameters with recrystallization time.

the recrystallization process comes to an end at about 400 min. The increase in the relaxation time could be ascribed to the decrease of the ionic mobility or to the lengthening of the route along which the charge carriers reciprocate as the internal structure builds up. The inference here is in accord with what Strobl [29] has proclaimed: spherulites are built up sequentially, starting with a rapid growth of dominant lamellae, which is then followed by an in-filling process running behind the growth front of growing spherulites. The Cole–Cole stretching exponent α shows a continuous decreasing trend. It means a continuous broadening of the MWS relaxation time distribution and implies the microstructure becomes more heterogeneous as recrystallization proceeds. PBSu has interesting recrystallization features which are dielectrically active. However, more studies are needed to elucidate the relationship between the dielectric behaviors and the morphological evolution.

4. Conclusions

PBSu exhibits complicated dielectric relaxation behaviors. At low temperatures (163–203 K), only the local β processes are observed. The much broader relaxation loss peak in the isothermal plot for the 363 K crystallized samples (compared to the quenched samples) leads to the speculation that it has a crystalline component. A well-defined α relaxation that originated from the segmental motion is not seen in the isothermal plot but can be well resolved in the isochronal plot. The α relaxation is obscured by the space charge effect, which becomes very pronounced at temperatures higher than 263 K. The spectra for temperatures higher than 303 K are totally dominated by DC conduction effect, interfacial MWS process and electrode polarization. The low temperature β process, DC conductivity and the MWS process all show an Arrhenius temperature dependence, while the α process exhibits an VFT dependence. The activation energies for the DC conductivity and the MWS process are identical, indicating they are of the same origin. A simultaneous melting and recrystallization scheme, which is usually employed to explain the multiple calorimetric melting behavior, is most evident in the 383 K spectrum. The fast melting and slow recrystallization allow us to observe clearly the spectroscopic evolution. The MWS relaxation time and strength and the distribution breadth increase with increasing recrystallization time, while the DC conductivity and the dielectric permittivity decrease. For these model parameters, the kinetic implication on recrystallization and the

relationship with microstructural evolution are not clear yet. However, they will be useful for exploring the recrystallization kinetics and microstructural development.

Acknowledgements

The author gratefully acknowledges funding from National Science Council of the Republic of China (Grants NSC 91-2216-E-214-005).

Appendix [19]

The equivalent circuit which represents the material in this present study consists of a Cole–Cole element in parallel with a capacitor and a resistor. The Cole–Cole element is chosen to represent the MWS polarization process. The capacitor represents the limiting high frequency MWS permittivity of the material, while the resistor represents the bulk conductance (resistance). The electrode polarization, which is resulted from the accumulation of charge carriers at the sample-electrode interface, is represented by a constant phase-angle (CPA) element. The overall measured admittance $Y_t(\omega)$ due to the combined admittance of the sample $Y_m(\omega)$, and the blocking electrodes, can be calculated considering the equivalent circuit made up by the series of $Y_m(\omega)$ with the CPA element $Y_e(\omega)$. The general expression for $Y_m(\omega)$ can be written as

$$Y_m(\omega)=\left\{j\omega\varepsilon_o\left(\varepsilon_\infty+\frac{\Delta\varepsilon}{(1+(j\omega\tau)^{\alpha})}\right)+\sigma_o\right\}\times\frac{S}{d}$$

where ε_o is the permittivity of free space, S and d are the sample surface and thickness, respectively, ε_∞ is the limiting high frequency MWS permittivity, $\Delta\varepsilon$ is the amplitude of the MWS polarization, α is the stretching exponent for the Cole–Cole element, τ is the median MWS relaxation time and σ_o is the bulk ionic conductivity. The complex admittance for a CPA element is expressed as

$$Y_e(\omega)=A(j\omega)^{\phi},$$

where A and ϕ are positive constants with $\phi\leq 1$. With $\phi=1$, the element behaves like a pure capacitor while with $\phi=0$, like a pure resistor. The total measured admittance is then expressed as:

$$Y_t(\omega)=\frac{Y_m(\omega)}{1+Y_m(\omega)/Y_e(\omega)}.$$

The measured admittance $Y_t(\omega)$ is directly related to the complex permittivity $\varepsilon^*(\omega)=\varepsilon'(\omega)-j\varepsilon''(\omega)$, given that

$$\varepsilon^*(\omega)=\frac{d}{j\omega\varepsilon_o S}Y_t(\omega).$$

References

[1] Fujimaki T. Polym Degrad Stab 1998;59(1–3):209–14.
[2] Ichikawa Y, Suzuki J, Washiyama J, Moteki Y, Noguchi K, Okuyama K. Polymer 1994;35(15):3338–9.
[3] Ichikawa Y, Washiyama J, Moteki Y, Noguchi K, Okuyama K. Polym J 1995;27(12):1230–8.
[4] Ichikawa Y, Kondo H, Igarashi Y, Noguchi K, Okuyama K, Washiyama J. Polymer 2000;41(12):4719–27.
[5] Ihn KJ, Yoo ES, Im SS. Macromolecules 1995;28(7):2460–4.
[6] Yoo ES, Im SS. J Polym Sci Polym Phys Ed 1999;37(13):1357–66.
[7] Qiu Z, Komura M, Ikehara T, Nishi T. Polymer 2003;44(26):7781–5.
[8] Yasuniwa M, Satou T. J Polym Sci Polym Phys Ed 2002;40(21):2411–20.
[9] Strobl G. The physics of polymers. 2nd ed. New York: Springer-Verlag; 1997.
[10] Roland CM, Ngai KL, Santangelo PG, Qiu XH, Ediger MD, Plazek DJ. Macromolecules 2001;34(18):6159–60.
[11] Boyd RH, Liu F. In: Runt JP, Fitzgerald JJ, editors. Dielectric spectroscopy of polymeric materials. Washington DC: American Chemical Society; 1997 [chapter 4].
[12] Fukao K, Miyamoto Y. J Non-Cryst Solids 1997;212(2-3):208–14.
[13] Neagu E, Pissis P, Apekis L, Gomez Ribelles JL. J Phys D Appl Phys 1997;30(11):1551–60.
[14] Malmstrom E, Hult A, Gedde UW, Liu F, Boyd RH. Polymer 1997;38(19):4873–9.
[15] Burshtein LL, Borisova TI, Zhukov SV, Nikonorova NA, Asinovskaya DN, Skorokhodov SS. Polymer 1999;40(7):1881–7.
[16] Tatsumi T, Ito E, Hayakawa R. J Polym Sci Polym Phys Ed 1992;30(7):701–6.
[17] Boyd RH, Aylwin PA. Polymer 1984;25(3):330–9.
[18] Zhang S, Jin X, Painter PC, Runt J. Macromolecules 2002;35(9):3636–46.
[19] Pizzitutti F, Bruni F. Rev Sci Instrum 2001;72(5):2502–4.
[20] Starkweather HW, Avakian P, Fontanella JJ, Wintersgill MC. Macromolecules 1993;26(19):5084–7.
[21] Mierzwa M, Floudas G, Dorgan J, Kanuss D, Wegner J. J Non-Cryst Solids 2002;307–310:296–303.
[22] Nogales A, Ezquerra TA, Garcia JM, Balta-Callaja FJ. J Polym Sci Polym Phys 1999;37(1):37–49.
[23] Lee YH, Bur AJ, Roth SC, Start PR, Harris RH. Polym Adv Technol 2005;16(2–3):249–56.
[24] Hedvig P. Dielectric spectroscopy of polymers. New York: John Wiley & Sons; 1977. p. 282–90.
[25] Macdonald JR, LEVMW software, Version 8.06. Downloaded from Solartron website: http://www.solartronanalytical.com/.
[26] Jorcin JB, Orazem ME, Pebere N, Tribollet B. Electrochim Acta 2006;51(8–9):1473–9.
[27] Druger SD, Nitzan A, Ratner MA. J Chem Phys 1983;79(6):3133–42.
[28] Bruce PG, Vincent CA. J Chem Soc Faraday Trans 1993;89(17):3187–204.
[29] Strobl G. Prog Polym Sci 2006;31(4):398–442.